International Journal of Earth Sciences (2024) 113:1457–1473
https://doi.org/10.1007/s00531-024-02448-0

ORIGINAL PAPER

# Imaging buried anticlines in the Po Plain, northern Italy, based on HVSR frequency and amplitude analyses

G. Tarabusi[1] · G. Sgattoni[1] · R. Caputo[2,3]

Received: 22 April 2024 / Accepted: 26 July 2024 / Published online: 6 August 2024


## Abstract

The use of the HVSR (Horizontal-to-Vertical Spectral Ratio) method on single-station microtremor measurements is well documented in small alluvial plains for bedrock mapping. In large sedimentary basins, like the Po Plain, its application is still debated. To shed some light on this issue, we investigated two seismogenic structures buried below the Po Plain Quaternary deposits: the Mirandola and Casaglia anticlines. We acquired and analysed a dense distribution of HVSR data covering the two areas and mapped the frequency and amplitude values of the observed resonance peaks. The top of both anticlines is highlighted by high amplitude peaks picturing E-W elongated sectors with high-impedance contrast, where Quaternary deposits are reduced in thickness to about 60–130 m and directly overlay the Pliocene (Mirandola) and Miocene (Casaglia) marine units. In Mirandola, the high-amplitude peaks also correspond to higher resonance frequencies, while in Casaglia, the distribution of resonance frequencies is relatively uniform suggesting a flatter crestal region and the lateral continuity of the resonance surface. The combination of peak frequency and amplitude information on a dense grid of measurement points is thus confirmed to be useful for identifying and mapping buried geological structures such as structural highs. Further modelling is being carried out to estimate the depth of the surface responsible for the observed resonances, through calibration with borehole information.

**Keywords** Seismic noise · Active tectonics · Seismic bedrock · Buried anticlines · Po Plain

## Introduction

The Po Plain represents the foredeep of two opposing fold-and-thrust belts, namely the north-verging Northern Apennines, to the south, and the south-verging Southern Alps, to the north. The frontal most sectors of both orogens are variably buried by the alluvial deposits of the plain. Among the hierarchically major structures of the Northern Apennines affecting the eastern sector of the Po Plain (Caputo and Tarabusi 2016) is the ca. 150 km-long faults-and-folds system of the Ferrara Arc (e.g. Vannoli et al. 2015). The most recent reactivations along this major tectonic feature have generated the May 2012 Emilia seismic sequence characterized by two main shocks, the 20 May, $M_w$ 6.1 and 29 May, $M_w$ 5.9 (*e.g.*, Pondrelli et al. 2012).

Notwithstanding the contractional tectonic activity affecting the region since Late Tertiary and persisting during Quaternary, and therefore the continuous shortening and growth of several fault-related folds, the Po Plain is characterized by substantially flat topography, highly contrasting with the subsoil stratigraphic architecture which is markedly structured into anticlines and synclines (*e.g.*, Pieri and Groppi 1981; Boccaletti et al. 2004; Maesano et al. 2015; Caputo and Tarabusi 2016; DISS Working Group 2021; Livani et al. 2023). As a direct consequence, the geological units filling the Po Plain foredeep show strong lateral thickness variations. For example, the Quaternary deposits in correspondence with the anticlinal hinges could be locally less than a hundred metres thick, while in the interposed synclines, the chronologically equivalent sedimentary succession could be as thick as some kilometres (*e.g.*, Bigi et al. 1992; Minarelli et al. 2016; Turrini et al. 2016). This general pattern is due to the synergistic role of overwhelming regional subsidence

✉ G. Tarabusi
gabriele.tarabusi@ingv.it

1 Istituto Nazionale Di Geofisica E Vulcanologia, Via Di Vigna Murata 605, 00143 Rome, Italy

2 Department of Physics & Earth Sciences, Ferrara University, Ferrara, Italy

3 CRUST, UR-UniFE, Ferrara, Italy

(*e.g.*, Cuffaro et al. 2010; Cenni et al. 2013; Severi et al. 2021) and a comparably high sedimentation rate characterizing the broader region, where even the more rapidly growing anticlines remain systematically buried and the associated faults always blind. At the surface, only subtle evidence of the presence at depth of these tectonic structures and their degree of activity could be inferred based on a meticulous examination of the hydrographic network allowing to recognize the presence of drainage anomalies (*e.g.*, Burrato et al. 2003, 2012).

The Mirandola and Casaglia anticlines are two of such buried fault-propagation folds that started forming during Quaternary due to the tectonic activity of blind thrust segments belonging to the wider Ferrara Arc (Fig. 1). These two tectonic structures represent the focus area of the present research. Indeed, in correspondence with the structural culminations of the fault-propagation anticlines characterizing the Mirandola, and Casaglia areas, the thickness of the continental Quaternary succession is highly reduced, being up to about 50 m in the Mirandola sector and 130 m in the Casaglia one, while Pleistocene deposits directly overlay the Pliocene and Miocene units, respectively (Boccaletti et al. 2004).

Unfortunately, the seismic reflection profiles were designed to target deep hydrocarbon deposits, and as such, the signal for the uppermost layers (as the ones corresponding to 200–400 ms) does not have high-quality, certainly with a vertical accuracy not suitable for reconstructing the shallower geometries. As a consequence, this technique can provide a picture of the subsoil down to several kilometres, but no information is generally, or rarely, available for the uppermost stratigraphic units, say the shallowest 100–300 m, which in turn would be of utmost importance for seismotectonic purposes by potentially documenting, for example, the occurrence of recent tectonic activity. On the other hand, the Po Plain subsoil has been diffusely explored by means of several geotechnical techniques. In this case, however, the corresponding investigation depth is commonly up to only few tens of metres, thus impeding regional scale correlations and hence to recognize with sufficient confidence the occurrence of tectonic signals generally characterized by much longer wavelengths (Caputo et al. 2015).

In order to better define the shallow geometry of the Casaglia and Mirandola folds, and hence possibly infer some evidence on the recent activity of the associated blind faults, we investigated the subsoil in a depth range which is intermediate between geotechnical investigations and deep seismic reflection profiles. To this aim, a well-known geophysical method, based on a passive seismic technique, has been systematically applied to both investigated areas, one of which corresponds to the 2012 epicentral area. Indeed, resonance frequencies are key parameters in seismic amplification studies (*e.g.*, Lermo and Chávez-Garcia 1994; Albarello et al. 2011; Mucciarelli 2011) and can be also used for stratigraphic reconstructions by relating them to the thickness and S wave velocity ($V_s$) of the resonating layers (*e.g.*, Ibs-Von Seht and Wohlenberg 1999; Parolai et al. 2002; Mantovani et al. 2019; Sgattoni et al. 2024).

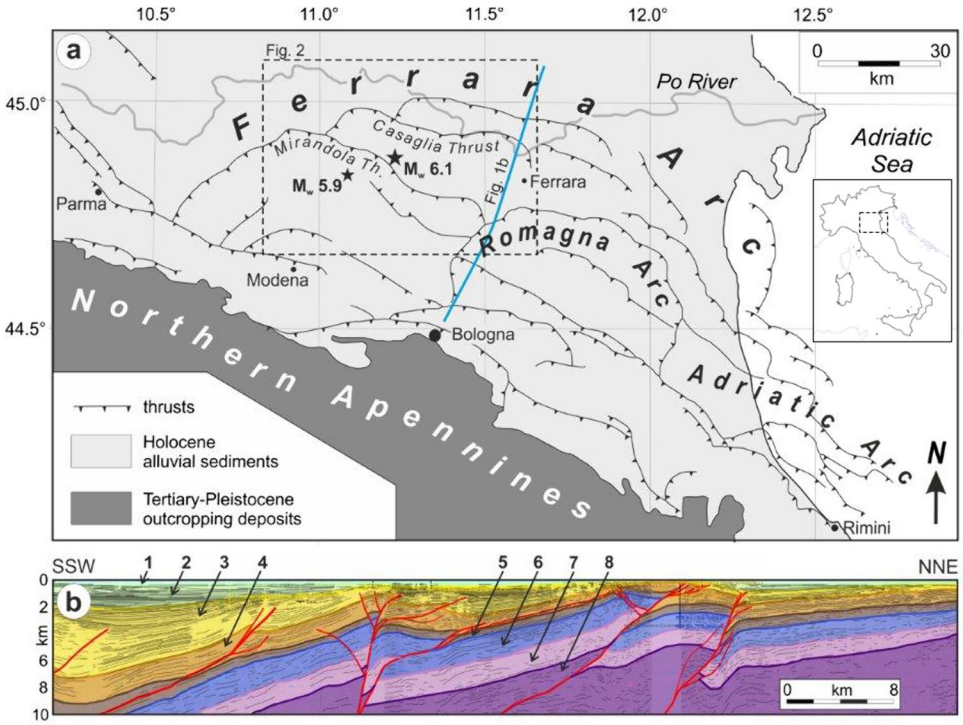


**Fig. 1** **a** Tectonic map of the buried Northern Apennines fold-and-thrust belt in correspondence with the eastern sector of the Po Plain. Modified from Bigi et al. (1992). The dashed box corresponds to the area shown in Fig. 2. The stars indicate the two major events of 20 (Mw 6.1) and 29 (Mw 5.9) May 2021, respectively. The blue line indicates the trace of the cross-section (b). **b** Section modified from Mistroni (2016). Legend: 1 Quaternary continental deposits; 2 Quaternary marine deposits; 3 Argille del Santerno Formation (Pliocene); 4 Miocene Formations; 5 Scaglia Formation (Eocene); 6 Cretaceous-Jurassic Formations; 7 Dolomia Principale (Triassic); 8 Permian basement

For the present research, a dense network of passive seismic acquisitions (Fig. 2) was carried out to obtain the horizontal-to-vertical spectral ratios (HVSR) to identify peak and secondary resonance frequencies. The followed approach has a twofold target: to develop a detailed subsoil model for the Casaglia area, and to improve a previously published one for the Mirandola area (Tarabusi and Caputo 2017). Based on the field measurements and their elaboration, high-resolution resonance frequency and HVSR peak amplitude maps and a 3D reconstruction of both anticlines have been produced. The results confirm the strong correlation between the HVSR outcomes, such as peak frequencies and amplitudes, and the stratigraphic architecture of the subsoil. These results also have several practical applications: firstly, they could contribute to identifying areas that are likely to experience greater ground motion amplifications during an earthquake; secondly, they enable the development of empirical formulas for estimating the depth of the seismic bedrock (i.e. $v_s \geq 800$ m/s), or the so-called pseudo-bedrock (i.e. $v_s \geq 600$ m/s), based on HVSR outcomes with high accuracy; and thirdly, this low-cost geophysical technique could highlight significant stratigraphic and structural differences between the Mirandola and Casaglia areas.

## Geological framework

The detailed stratigraphic succession of the Po Plain has been basically reconstructed by borehole data and, above all, by several reflection profiles carried out for hydrocarbon explorations, currently only partially available online (ViDEPI Project, https://www.videpi.com). As mentioned above, the available stratigraphic data show that the thickness of the Pleistocene sedimentary succession is significantly reduced in correspondence of the two investigated anticline areas. As a regional stratigraphic reference, at least in the syncline areas where the sedimentary succession is virtually continuous, we can assume the general scheme of the central part of the Po Basin proposed by the GeoMol Team (2015) and consisting of the following principal units (Fig. 3).

Pleistocene units are identified by several surfaces corresponding to minor unconformities, well developed especially at the Apennines margin and therefore very useful to constrain the tectonic evolution of the buried structures; the QC1 horizon separates the overlying continental deposits ("PLC", clay, silt and sand), from the underlying marine and transitional ones ("PLM", mainly sand and silt, locally gravel).

Pliocene units are composed of marine shale and sand deposits, including locally fine-grained turbidites. They are subdivided into the following units: Porto Corsini Formation, Porto Garibaldi Formation and Argille del Santerno Formation ("PL").

Miocene units consist of gravel and sand deposits developed in marine deltaic fans belonging to the Sergnano Formation and Fusignano Formation ("MESb"), silt deposits with evaporites (marine transitional environment) of the Gessoso Solfifera Formation ("MESa") and marl, sand and locally gravel of Marne di Gallare Formation ("MESa" and "MIO"). Relative to the Mirandola and Casaglia sectors, two high-resolution sections (Fig. 4a and b) based on

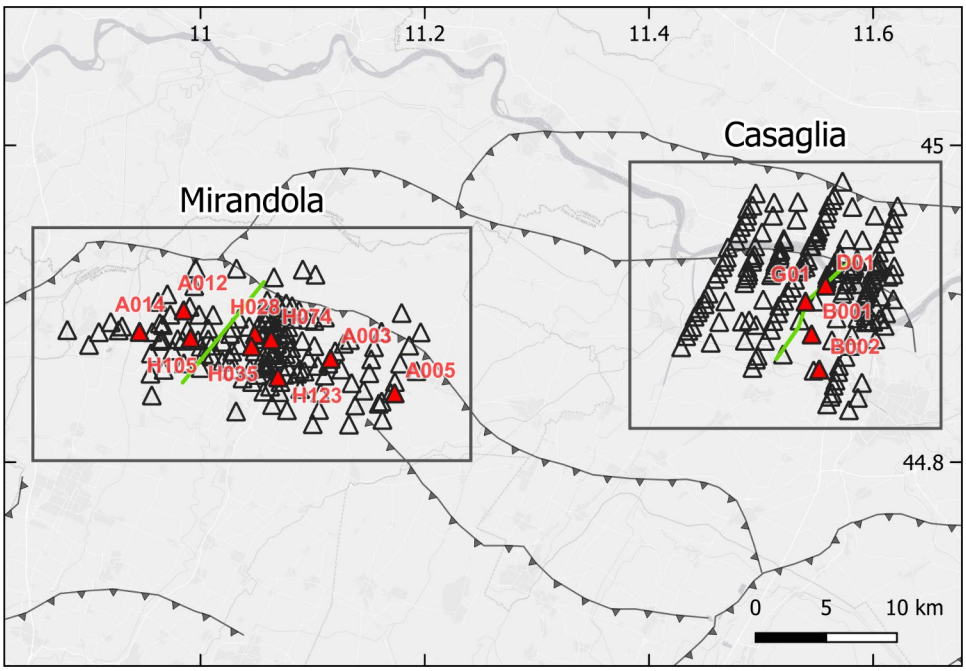


**Fig. 2** Map of the investigated areas showing the traces of the main buried thrusts and the HVSR measurements (triangles) carried out in Mirandola and Casaglia sectors. Red triangles represent HVSR sites close to boreholes for which lithostratigraphy is available. This information was crucial for obtaining the peak frequency *versus* depth empirical relationship (Table 1). Green lines indicate the traces of the two cross sections represented in Fig. 4a and b

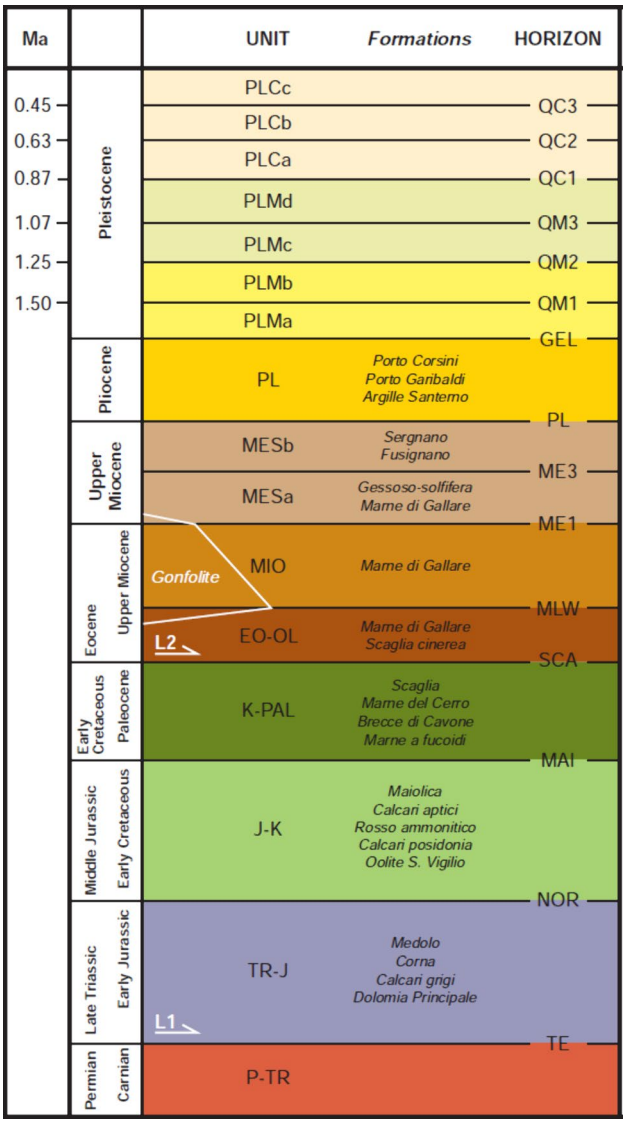


**Fig. 3** Stratigraphic column of the central part of the Po Basin (from GeoMol Team 2015), with only main formations listed

hydrocarbon exploration data and other core drilling data, were recently published (Martelli 2021). Moreover, for the purpose of the present research, we were able to inspect a set of ten hydrocarbon borehole logs performed in both investigated areas as well as three boreholes drilled by Regione Emilia-Romagna down to the geological substratum of the alluvial deposits (two in the Mirandola area and one in the Casaglia area). For the latter three boreholes, carried out for seismic microzonation studies, a detailed stratigraphic log is available, and the $V_s$ was measured with cross-hole tests (Martelli 2021). Simplified logs of five selected boreholes in the hinge zone of both investigated areas are shown in Fig. 4c.

## HVSR data and method

Microtremor (or background noise) is ubiquitous at the Earth's surface and associated with many different natural phenomena and/or anthropogenic activities. It is generally characterised by very small oscillations with spectral components poorly attenuated in space and measurable with passive recording techniques. Elastic waves always suffer geometric attenuation due to the widening wavefront, but also intrinsic attenuation due to the partially anelastic behaviour of all rocks. In both cases, the amount of attenuation is a function of frequency. Indeed, assuming a constant velocity, the shorter the wavelength (*i.e.* the higher the frequency) the greater the number of cycles and hence the attenuation occurred. Accordingly, stratigraphic layering governs the distribution of the mechanical properties (*e.g.* Castellaro et al. 2005). Such information is included in the recorded microtremors together with random noise, and it can be extracted by means of several methods like the one proposed by Nakamura (1989; horizontal to vertical spectral ratio, HVSR). This technique is nowadays largely used in order to determine the local seismic amplification and to estimate the principal resonance frequencies of the shallow subsoil, say from tens to some hundreds of meters, being both parameters of utmost importance for anti-seismic engineering planning.

The HVSR method involves recording microtremors with a single three-component seismometer and calculating the ratio of the horizontal and vertical Fourier amplitude spectra. The interpretation of microtremor HVSR is complicated by the unknown composition of the microtremor wavefield, which also varies with frequency and from site to site. Whether the wavefield composition is mainly body waves, surface waves, or a combination of them, is still debated (e.g. Bonnefoy-Claudet et al. 2006; Sánchez-Sesma 2017). Moreover, some methods exist to separate specific wave components to calculate and invert HVSR (e.g. Mi et al. 2019). However, whatever the nature of microtremors, there is general consensus on the fact that a major peak in the HVSR curve occurs at the resonance frequency of the subsoil, which depends on the presence of a mechanical discontinuity along the vertical of the measured site (see Molnar et al. 2022 for a review of the HVSR method).

Following this methodological approach, we carried out two major field campaigns. In particular, the results of a previous study performed in correspondence with the Mirandola anticline area (Tarabusi and Caputo 2017) represent a starting point of this research, in which we largely increased the original dataset and extended the method to the area of the Casaglia anticline, where the stratigraphy and the relationships between the subsoil units are similar though partly different.

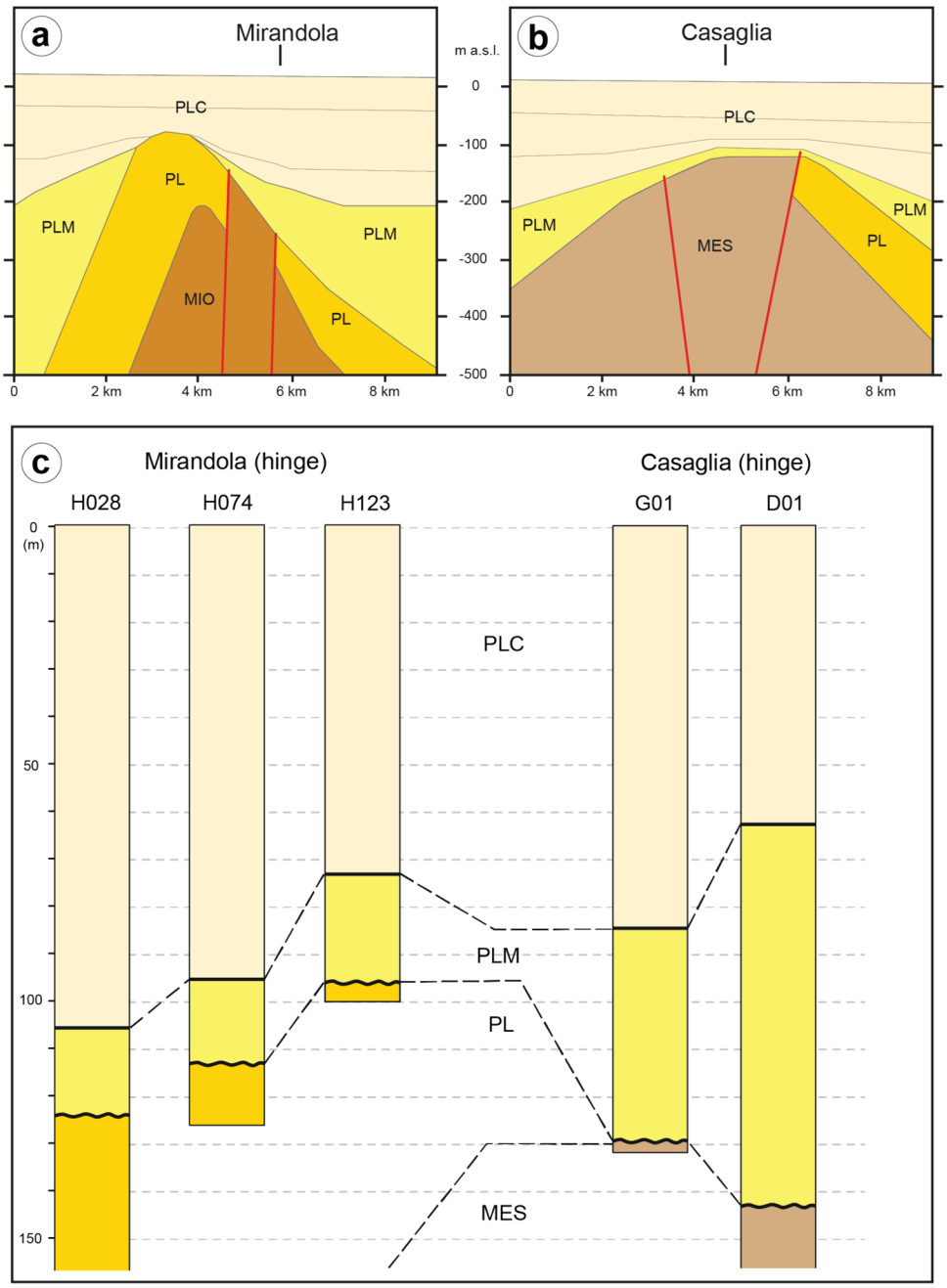


**Fig. 4** Geological sections across the Mirandola (**a**) and Casaglia (**b**) anticlines (Martelli 2021). Selected borehole logs from both investigated areas used to fix the bedrock depth in the hinge zone and, hence, to calibrate the HVSR measurements carried out nearby these sites (**c**)

## Acquisition and processing

We analysed a set of 326 single-station microtremor measurements acquired in the Mirandola (151) and Casaglia (175) areas (Fig. 2), following as a standard the well-tested SESAME criteria (Bard et al. 2005). The data were acquired with Tromino seismometers (MoHo srl) at 128 Hz sampling rate and lasted 12 to 40 min. All measurements were acquired in free-field conditions as far as possible from buildings. The data were acquired with four different instruments and several measurements were repeated at the same site to check their repeatability and the temporal stability of the results. Part of the data used in this study for the area of Mirandola (131 measurements) were collected by Tarabusi and Caputo (2017). Whatever the case, all these measurements have been (re)analyzed in the frame of this research to have uniformity and for a better definition of peaks and amplitudes, this explaining slight differences from the previously published ones.

Grilla software (Castellaro and Mulargia 2009) was used to obtain HVSR curves. Each waveform was split into 30 s non-overlapping windows, detrended, tapered, padded, FFT-transformed and smoothed with triangular function with a width equal to 10% of the central frequency. We

then obtained HVSR curves for each measurement site by averaging the HVSR computed for each time window, after manually removing windows contaminated by transients and artefacts in the frequency domain. The horizontal amplitude, $H$, has been computed as the geometric average of the two horizontal components of motion. The resulting HVSR curves are presented in terms of average among the different windows and the corresponding standard deviation. Examples are shown in Fig. 5, while all numerical values are attached in the Supplementary Material.

## Analytical approach

The main resonance frequencies of the ground can be identified as peaks on the HVSR curves. When several impedance contrasts are present in the subsoil, several peaks are also observed in the HVSR curves (Oliveto et al. 2004; Tarabusi and Caputo 2017; Mantovani et al. 2019). To identify our target resonances, *i.e.* the peaks associated with the anticline structures, we analysed HVSR curves along transects enabling us to laterally correlate resonance peaks at the different measurement sites We first analysed individual HVSR curves in conjunction with their individual spectral components of motion (Fig. 5). This allowed for distinguishing stratigraphic *versus* anthropogenic peaks (Castellaro 2016) and discerning the 1D/2D nature of the measured signal at the site (Sgattoni and Castellaro 2020; Sgattoni et al. 2023).

Subsequently, we combined the HVSR curves obtained along the transects into contour plots interpolated as a function of distance and colour-coded for HVSR amplitude (Fig. 6), using a natural-neighbour interpolation algorithm. These graphs represent 2D pseudo-sections where dark red highlights resonance peaks and their frequency variations with distance along the transect (Mantovani et al. 2018). They were drawn using HVSR curves with their original absolute amplitudes (Fig. 6b) and individually normalized by the maximum at each site (Fig. 6c). Accordingly, the plots with normalized amplitudes highlight lateral changes

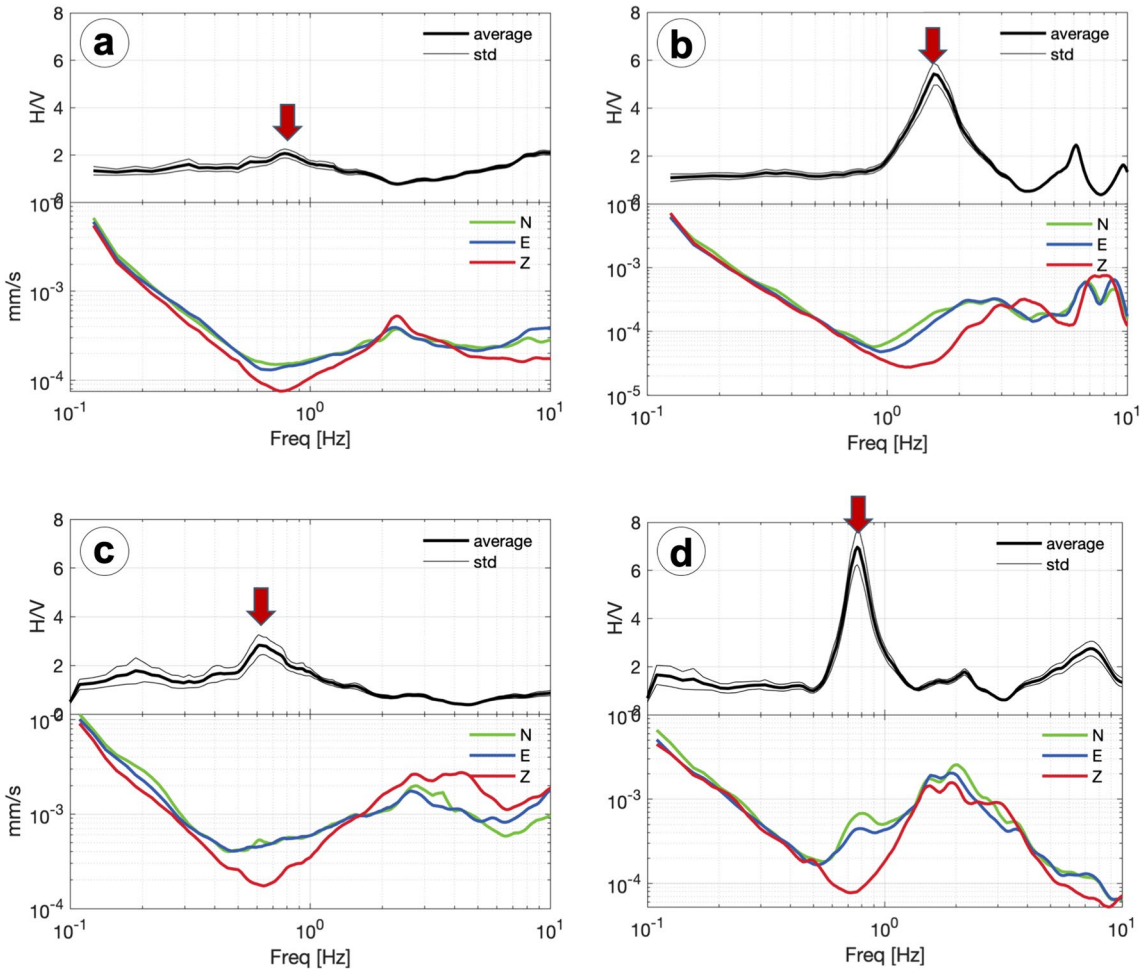


**Fig. 5** Examples of HVSR curves and individual spectral components of motion acquired in Mirandola (**a** and **b**) and in Casaglia (**c** and **d**). In **a** and **c** the HVSR peak is low-amplitude and wide, while in **c** and **d** the HVSR peak is high-amplitude and narrow

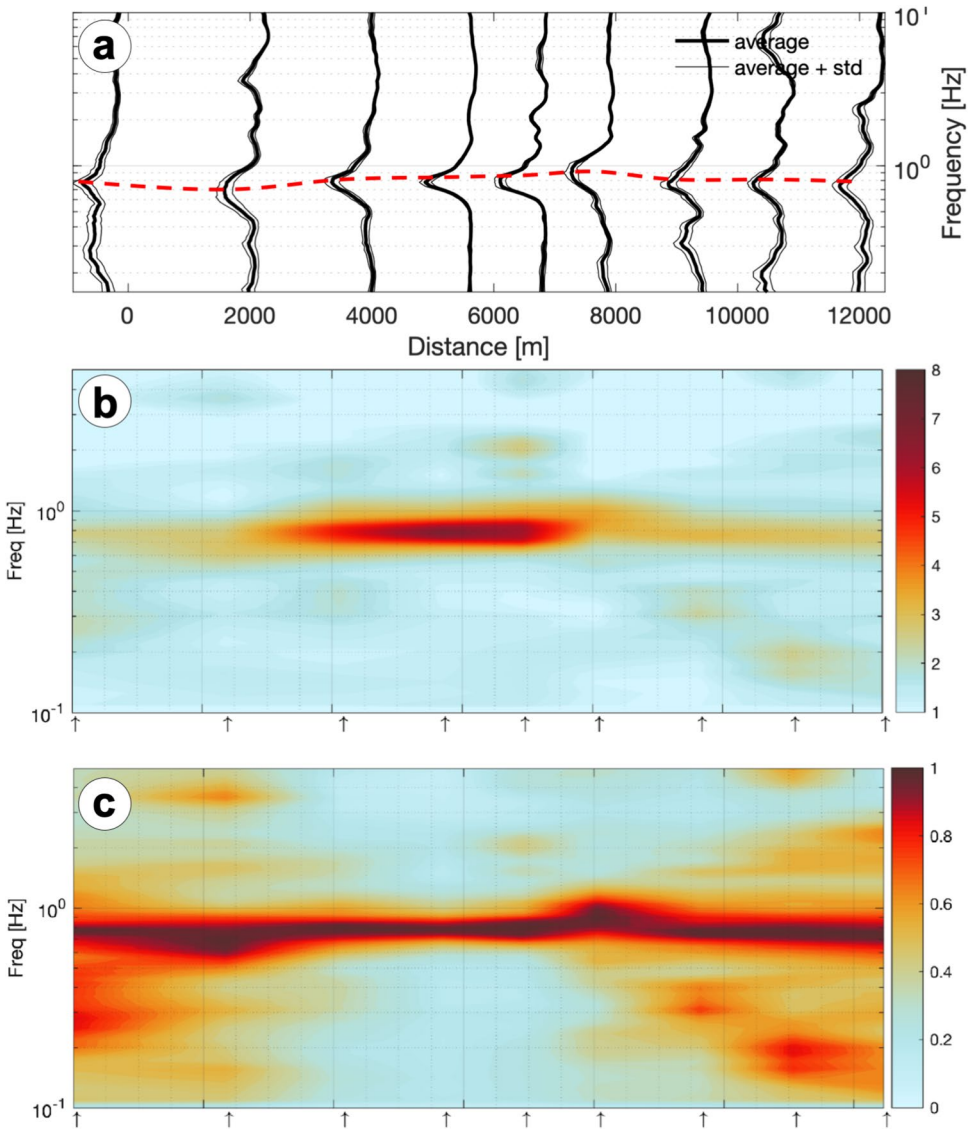


**Fig. 6** Construction of HVSR contour profiles. **a** HVSR curves plotted as a function of distance along a transect. The red dashed line connects adjacent resonance peaks. The same HVSR curves have been laterally interpolated in terms of absolute values of the peak amplitude (**b**) or based on amplitudes individually normalized by each HVSR curve's maximum (**c**)

in resonance frequencies, while plots with absolute amplitudes highlight lateral changes in peak amplitudes. As further discussed in a following section, the integrated analysis of both plots provides useful information to identify the anticline structures in the two investigated areas (Figs. 7 and 8). The interpolated transects with normalized amplitudes of Figs. 7c and 8c highlight more clearly the lateral variations occurring in resonance frequency values.

## HVSR peaks analyses

We extracted the frequency and amplitude values of all HVSR resonance peaks associated with the anticline top surface in both study areas. This operation was performed with an automatic procedure coded into a Matlab script, designed to look for peaks in the HVSR curves and to select those located within the frequency range of interest (0.5 to 2 Hz in our case). The HVSR peak frequencies and amplitudes have been thus automatically identified at all 326 sites (see the tables attached in the Supplementary Material). With these values, we then created two colour-coded maps representing the distribution of the peak amplitude and peak frequency in both investigated areas (Figs. 9 and 10).

It is worth to mention that the HVSR resonance peaks tend to be high-amplitude and narrow (Fig. 5b and d) especially in the central sector of both investigated areas, and much lower and wider in the outer areas (Fig. 5a and c). This is also clearly visible in the contour plots represented in Figs. 9b and 10b, where HVSR amplitudes are represented with their absolute values. It is worth to note that the maximum observed HVSR amplitudes are close to 8 in Casaglia, and 6 in Mirandola.

From the comparison between Figs. 9 and 10, it is possible to observe that the greater amplitudes of the peaks are

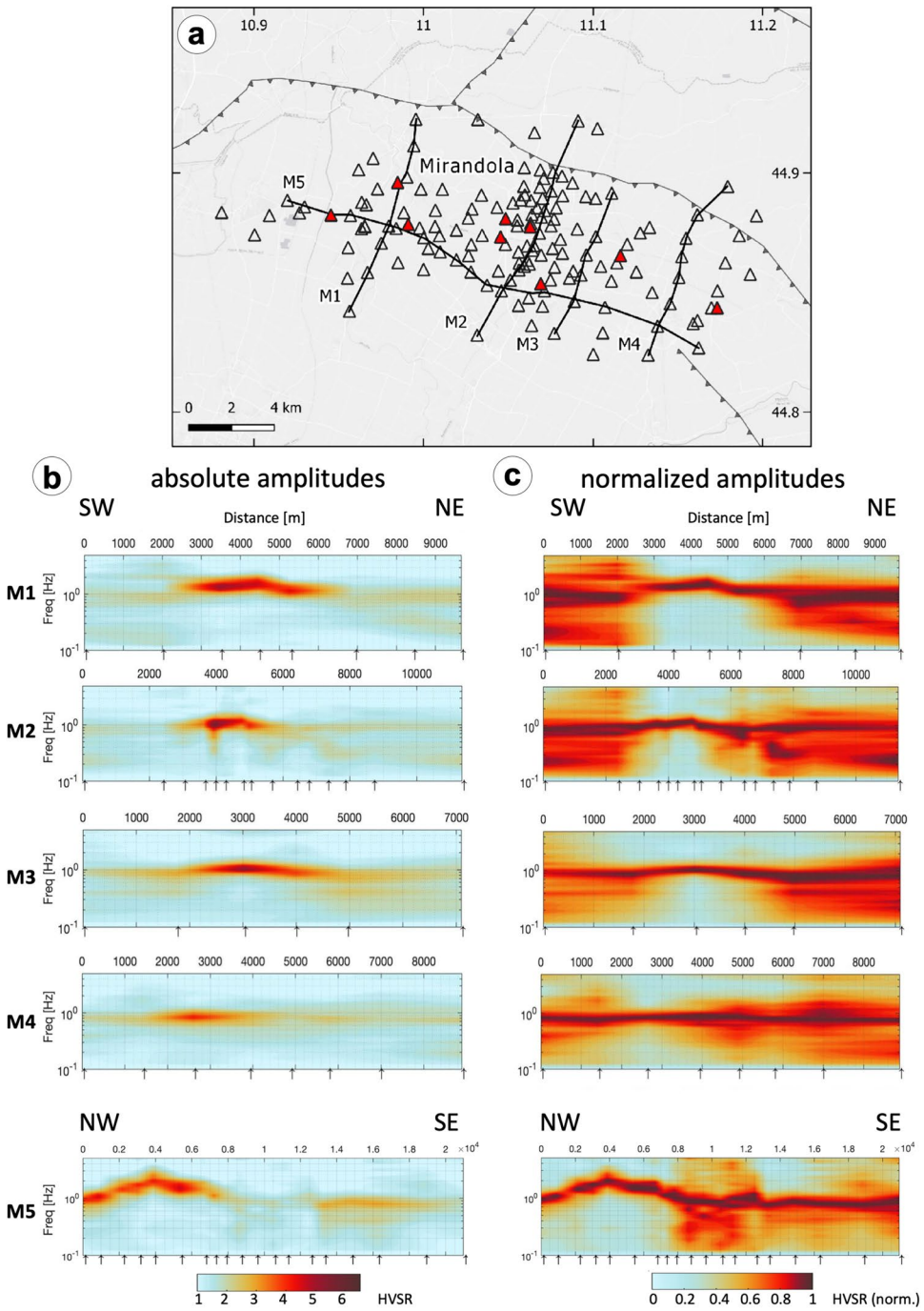


**Fig. 7** Interpolated amplitude HVSR profiles across the Mirandola area (**a**) based on the absolute values (**b**) and normalized ones (**c**). Profiles labels are shown in (**a**)

concentrated in the central portion of both areas suggesting an ESE-WNW trend. However, only in the Mirandola area, the pattern of the frequencies of the maximum peaks mimic that of the amplitudes, while this does not occur in the Casaglia area, where peak frequencies slightly increase only locally.

The maps document the presence, in both areas, of prominent sectors characterized by large resonance phenomena, testified by high-amplitude resonance peaks. In the Mirandola area, the larger amplitude values also correlate with the higher resonance frequency values, highlighting the presence of a relatively narrow and marked hinge zone of the buried anticline (Fig. 9). In the Casaglia area, instead, the frequency distribution is relatively uniform, while a clear E-W trending high-amplitude ellipse-shaped area is clearly emphasized by the amplitudes distribution (Fig. 10). The difference in the peak frequency *versus* amplitude distribution between in the two study areas is outstanding in Fig. 11. Indeed, a general correlation between peak frequency and peak amplitude is clearly observed in the Mirandola dataset,

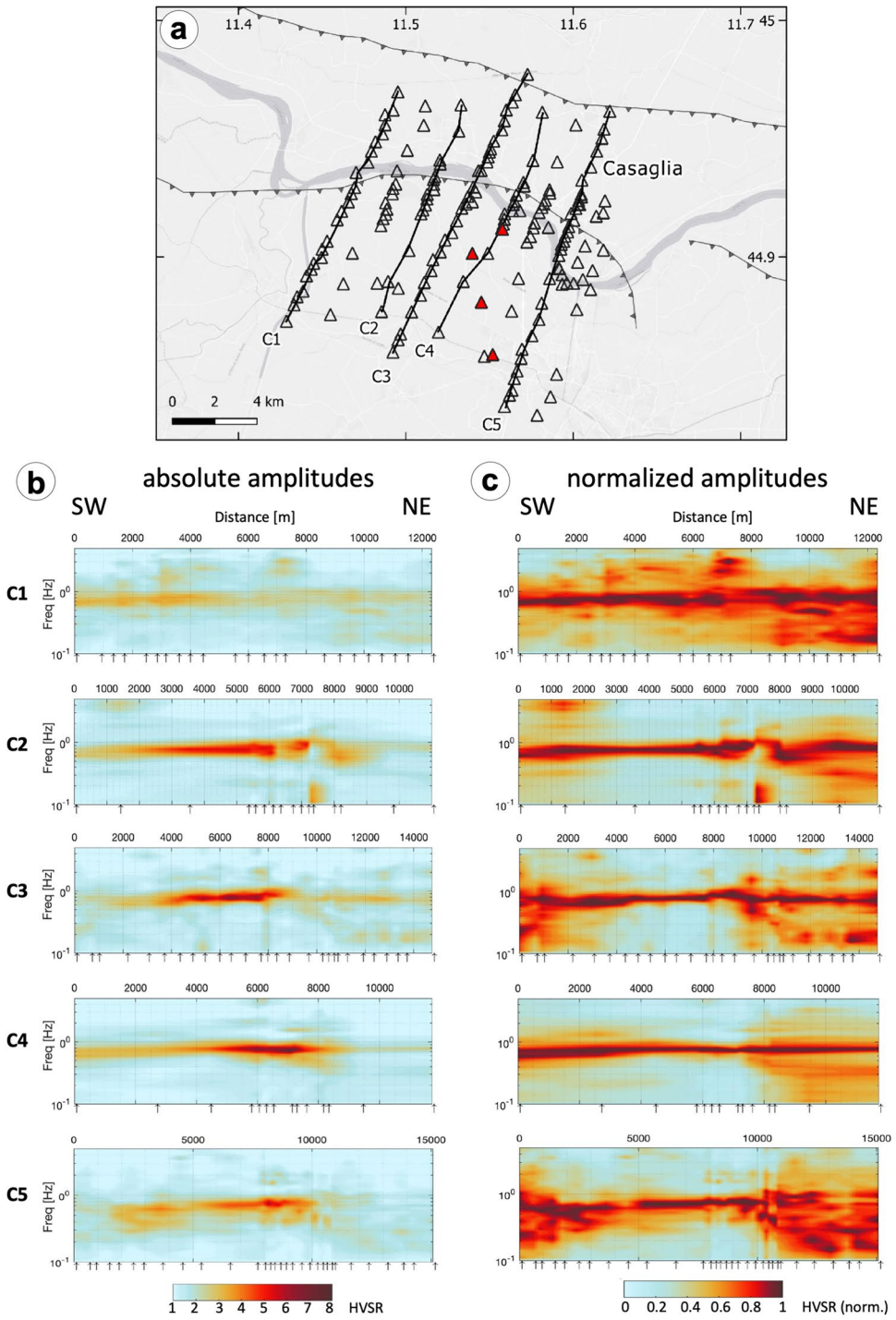


**Fig. 8** Interpolated amplitude HVSR profiles across the Casaglia area (**a**) based on the absolute values (**b**) and normalized ones (**c**). Profiles labels are shown in (**a**)

while in Casaglia a large range of peak amplitudes correspond to fairly constant frequency values.

In this regard, it is likely that the observed high amplitudes (Figs. 9b and 10b) are due to marked resonance phenomena, sharply decreasing both northwards and southwards. We interpret the highest amplitude values and the general trend in the two maps as a result of laterally changing impedance contrast occurring within the uppermost stratigraphic succession. The highest values are observed on top of the Mirandola and Casaglia anticlines, where the thickness of the continental Quaternary deposits is generally reduced (less than 100 m in Mirandola and about 130 m in Casaglia) and they directly overlay the Pliocene (Mirandola) and Miocene (Casaglia) marine units, respectively. The similarity of the sedimentary succession overlying the unconformity and the different units characterizing the underlying

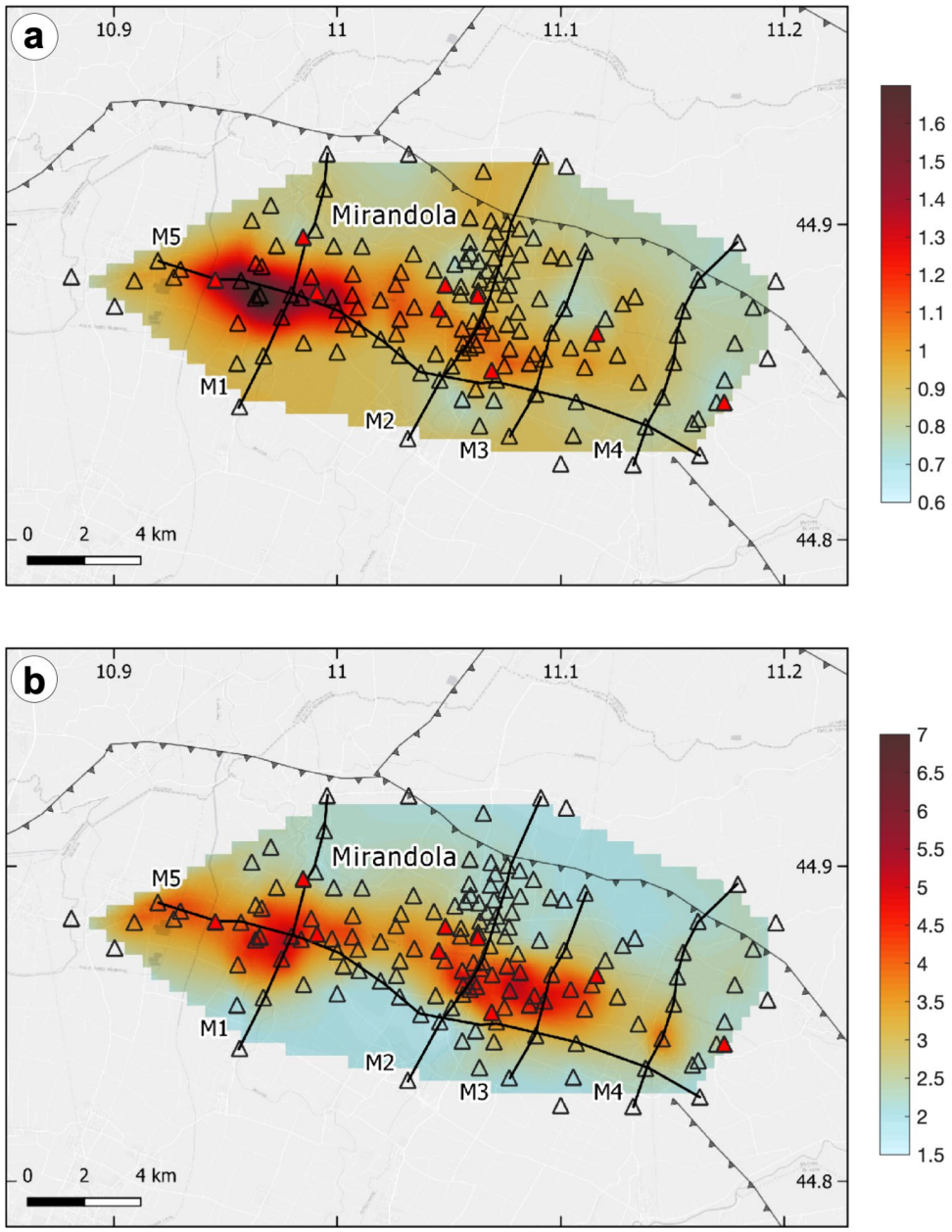


**Fig. 9** Map of the HVSR peak frequency (**a**) and amplitude (**b**) of the Mirandola area based on the single-station microtremor measurements (triangles)

rock volume, determines a contact with a greater impedance contrast in Casaglia and, therefore, explains the higher local amplitude values measured there. In summary, this different pattern likely suggests the occurrence of a flatter and wider crestal region in the Casaglia area and the lateral continuity of the same resonance surface within the conterminous synclines, though with a much lower impedance contrast.

## Depth conversion

In order to further analyse the obtained results, we attempted to convert the HVSR profiles from the frequency domain to the spatial domain by applying the 1D resonance equation which relates the fundamental ground resonance frequency ($f_0$) with the S-wave velocity ($V_s$) and the thickness ($h$) of the resonating layer:

$$f_0 = V_S/4h \quad (1)$$

The application of this equation requires i) the assumption of 1D site conditions at each measurement site, and ii) a $V_s$ model for the sedimentary layer overlying the contrast surface. The 1D assumption is verified in both study areas for the resonance frequencies of interest as far as possible lithological and, hence, mechanical lateral variations are characterized by greater wavelengths relative to the expected

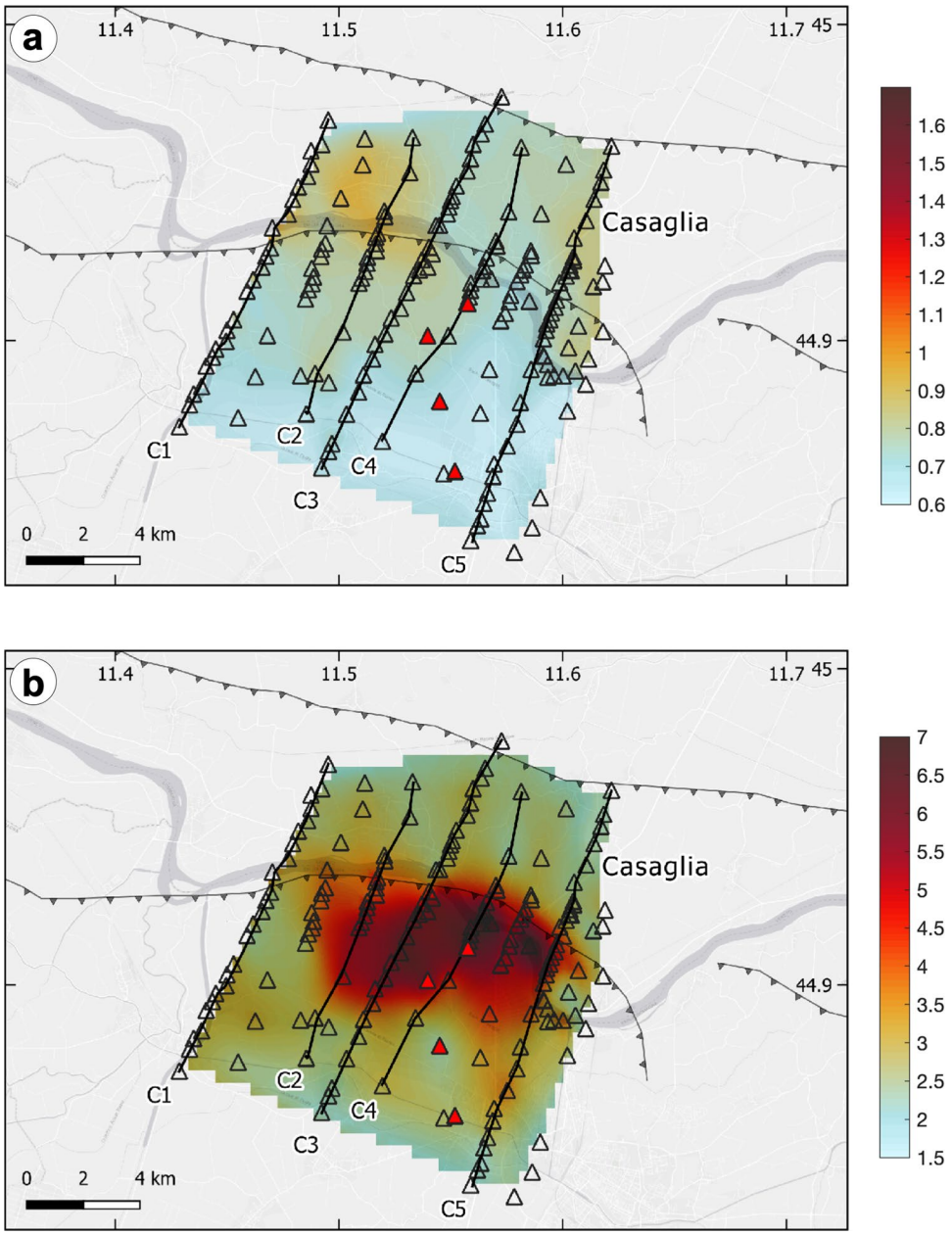


**Fig. 10** Map of the HVSR peak frequency (**a**) and amplitude (**b**) of the Casaglia area based on the single-station microtremor measurements (triangles)

vertical dimension of the sedimentary unit. The features of HVSR peaks considered for the depth conversion meet the 1D condition described in Sgattoni and Castellaro (2020), i.e. a local trough is observed in the vertical spectrum and horizontal spectra coincide around the resonance frequency. We note that Eq. (1) was applied considering the main resonance peak on each HVSR curve. At sites where secondary peaks exist, these are at lower frequencies and, therefore, represent deeper impedance contrasts. These are not considered in this study because they are less important for engineering applications, often lack spatial continuity, and are more problematic to be interpreted due to the large depths they represent.

As concerns the $V_s$ velocity model, it can be derived by correlating the observed resonance frequencies with known depths of impedance contrasts directly observed in boreholes (*e.g.*, Ibs-von-Set and Wohlemberg 1999). To this purpose, we carefully analysed all microtremor data acquired near to 13 sites where borehole data are available, and we identified the stratigraphic surfaces that correlate with their corresponding resonance peaks. Two examples of stratigraphic-HVSR curve correlation are also reported in Fig. 12. The resulting frequency-depth paired values at the constraint sites are reported in Table 1 and represented in Fig. 13. As shown in Fig. 13, the data from

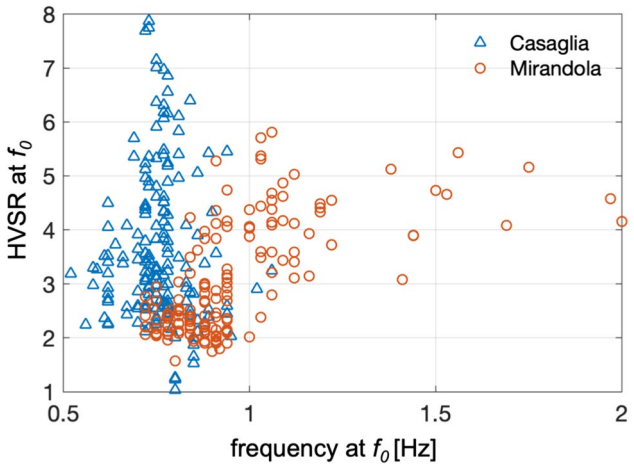


**Fig. 11** Distribution of the HVSR peak amplitudes *versus* frequencies at both investigated areas

the 13 available boreholes allowed for a good correlation between HVSR peaks and stratigraphic surfaces.

By assuming a power-law relation for the increasing $V_s$ with depth, a peak frequency *versus* depth empirical relationship can be derived by fitting measured resonance frequencies with the identified substrate depths. This method was first proposed by Ibs-von Seth and Wohlemberg (1999) and has been used by several authors in several valley contexts (*e.g.*, Parolai et al. 2002; Özalaybey et al. 2011; Paolucci et al. 2015; Tün et al. 2016; Mantovani et al. 2018; Sgattoni et al. 2024).

Initially, separate regression analyses were conducted for the two areas of Mirandola and Casaglia, which yielded very similar results; therefore, the regression analysis that we propose was conducted jointly for the two areas, as shown in Fig. 13. The obtained frequency, *f*, *versus* depth, *h*, relation is the following:

$$h = 100f^{-1.28} \tag{2}$$

This empirical relationship is valid for the shallow subsurface within the depth range used for the regression analysis (from − 60 to − 230 m), which allows the conversion from the frequency to the depth domain of the HVSR curves. The available data show a very good fit, being the coefficient of determination $R^2$ equal to 0.99 and the mean absolute error of about 5 m.

## Discussion

The opportunity to compare the distribution of frequency and amplitude values with reliable stratigraphic data on the basis of 13 deep boreholes and with the available geological sections (Fig. 4a and b) and the application of this information to all the HVSR results previously described is particularly important for the purposes of this research. Indeed, this allowed (i) to correlate the type of observed peaks with the depth and nature of the stratigraphic surfaces associated with the impedance contrast; (ii) to establish a regression model between frequency and depth and subsequently a velocity model enabling to estimate the depth of the seismic bedrock, or pseudo-bedrock, in the broader study areas; (iii) to verify whether the different nature and distribution of HVSR peaks in the two investigated areas are closely related to the different structure of the two anticlines.

By applying the obtained regression equation to all HVSR curves and by simple interpolation, it was possible to reconstruct the geometry at the depth of the 'resonant surface' for both areas (Fig. 14) from which the following considerations could be made. Firstly, as for the Mirandola area (Tarabusi and Caputo 2017), also for Casaglia a high impedance contrast occurs due to the abrupt increase of material density and hence of seismic wave velocity. This is in correspondence with the structural culminations of the fault-propagation anticlines, where the thickness of the continental Quaternary deposits is generally reduced, and they overlay directly the Pliocene or Miocene units in the Mirandola and Casaglia areas, respectively. Secondly, as previously highlighted, the Casaglia anticline, unlike the Mirandola one, seems not to affect the HVSR frequencies with a well-defined pattern (Fig. 10a), though it is clearly depicted in the map view based on the amplitude values (Fig. 10b). A possible explanation for this is that the frequency (and therefore the depth) of the surface that generates the (major) impedance contrast in correspondence of the Casaglia anticline hinge (about 0.7 Hz) roughly coincides with a different stratigraphic surface located within the Quaternary sequence in the surrounding areas of the Po Plain (about 0.7 Hz, but with lower amplitude values; Mascandola et al. 2019). Thirdly, the maximum HVSR peak amplitudes are higher in Casaglia (up to 8) than in Mirandola (up to 5). This reflects a higher impedance contrast in Casaglia, that could be attributed to a different bedrock age, being Miocene in Casaglia and Pliocene in Mirandola, and therefore the corresponding overall mechanical competence. Fourthly, in both areas, in correspondence with the limbs of the anticlines, where the surface responsible for the main impedance contrast is likely 'QC1', between continental and marine Pleistocene deposits (Fig. 3), the peaks show low amplitudes (generally less than 3); conversely, in folds culmination, where the main impedance contrast is caused by Pliocene (Mirandola) or Miocene (Casaglia) deposits, the peaks show higher values (more than 3) (Fig. 12).

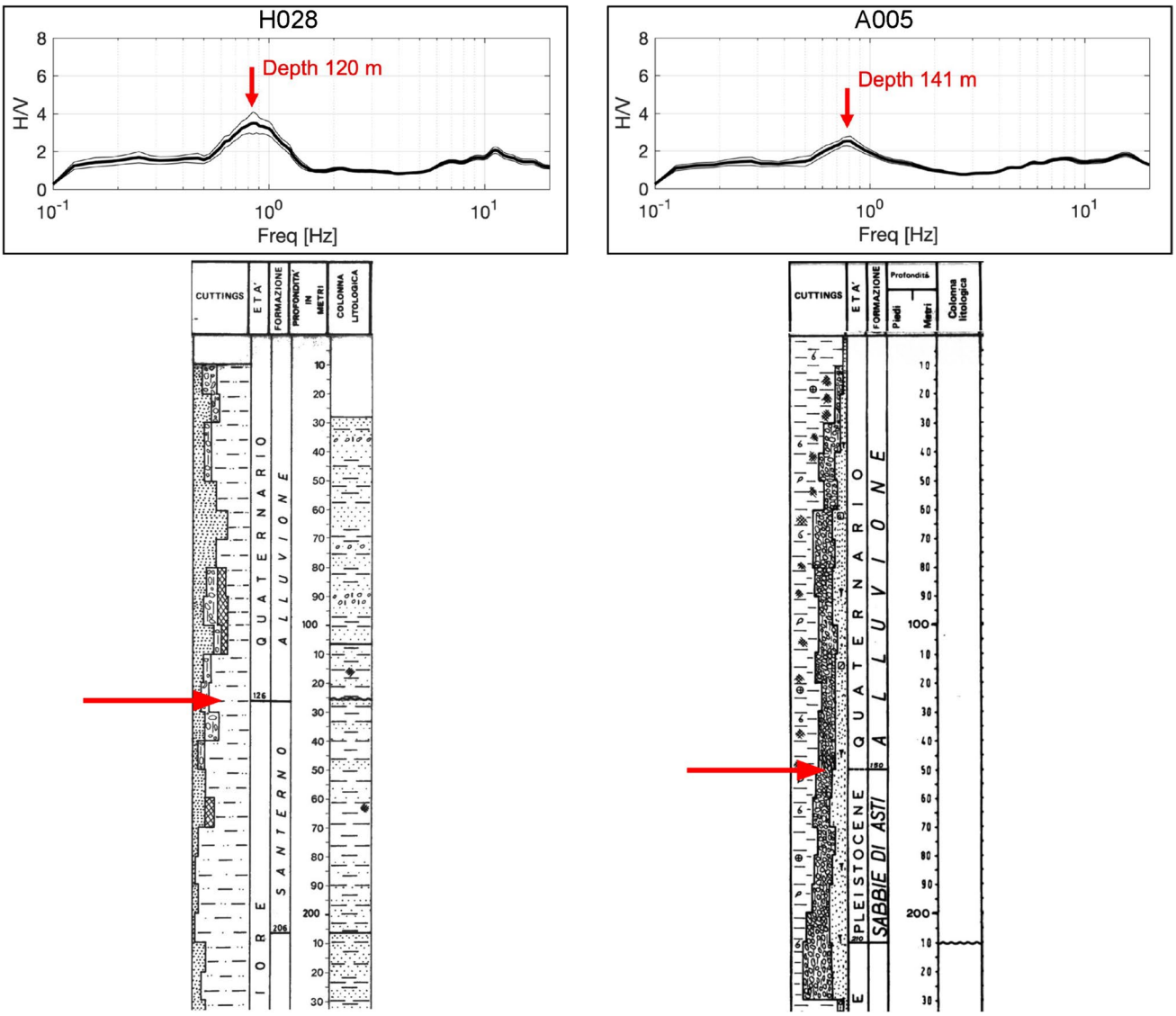


**Fig. 12** Examples of correlation between HVSR curves and stratigraphic surfaces drilled in hydrocarbon boreholes. The depths of the 'resonant' surface and the frequencies of the peaks show a good agreement, though in H028 the reflector corresponds to the Pleistocene-to-Lower Pliocene stratigraphic discontinuity and in A005 the reflector is the "QC1" surface (Fig. 3) separating continental and marine Pleistocene deposits. Note also that in the former case, in correspondence of bedrock, the amplitude is about 3.5, while in the latter, in correspondence of pseudo-bedrock, it is only 2.5

## Concluding remarks

HVSR amplitudes are influenced by several factors, like seismic noise amplitude and wave content (Nakamura 1989), impedance contrast (Ibs-von Seht and Wohlenberg 1999), 2D resonance mode shapes (Ermert et al. 2014; Sgattoni and Castellaro 2020; Sgattoni et al. 2023) and velocity inversions (Castellaro and Mulargia 2009). This implies that the direct use of HVSR peak amplitudes for, *e.g.*, estimating the amplification factors is not straightforward. On the other hand, the analysis of the spatial distribution of HVSR peak amplitudes carries useful information when the origin of the HVSR peak is instead well-defined (stratigraphic, 1D/2D, etc.).

The results of the present study show and confirm how the systematic application of the HVSR method over a relatively dense grid of measurements covering a wide area allows the identification, for example, of folded surfaces, other tectonic features and/or the bedrock geometry buried in the shallow subsoil (Moisidi et al. 2015; Tűn et al. 2016; Mantovani et al. 2019; Khalili and Mirzakurdeh 2019; Yamada et al 2020; Famiani et al. 2022). In our case studies, the spatial patterns of $A$ and $f_0$ in correspondence with the Mirandola and Casaglia anticlines nicely fit the available geological

**Table 1** Constraint points used for frequency-depth relation: HVSR measures acquired near sites where borehole data are available

| HVSR measure | | | | | Area | Borehole | | |
|---|---|---|---|---|---|---|---|---|
| Label | lat | lon | $f_0$ | $A$ | | Type | Depth [m] (surface) | Unit (bedrock or pseudo-bedrock) |
| A003 | 44.8654 | 11.1160 | 0.91 | 2.9 | Mirandola (hinge) | H | 106 | PL |
| A005 | 44.8436 | 11.1731 | 0.79 | 2.5 | Mirandola (limb) | H | 141 | PLM |
| A012 | 44.8960 | 10.9848 | 0.74 | 2.6 | Mirandola (limb) | H | 156 | PLM |
| A014 | 44.8824 | 10.9455 | 1.44 | 3.9 | Mirandola (hinge) | H | 62 | PL (Porto Garibaldi) |
| B001 | 44.8808 | 11.5451 | 0.67 | 2.4 | Casaglia (limb) | H | 173 | PLM |
| B002 | 44.8586 | 11.5519 | 0.62 | 2.8 | Casaglia (limb) | H | 192 | PLM |
| D01 | 44.9117 | 11.5577 | 0.77 | 6.3 | Casaglia (hinge) | H | 143 | MESa (Gessoso Solfifera) |
| G01 | 44.9015 | 11.5397 | 0.78 | 6.2 | Casaglia (hinge) | R | 130 | MES (Undefined) |
| H028 | 44.8809 | 11.0484 | 0.84 | 3.5 | Mirandola (hinge) | H | 120 | PL (Argille del Santerno) |
| H035 | 44.8732 | 11.0454 | 1.09 | 3.4 | Mirandola (hinge) | H | 91 | PL (Porto Garibaldi) |
| H074 | 44.8775 | 11.0629 | 0.86 | 3.6 | Mirandola (hinge) | R | 114 | PL (Undefined) |
| H105 | 44.8785 | 10.9910 | 1.44 | 3.9 | Mirandola (hinge) | H | 65 | PL (Porto Garibaldi) |
| H123 | 44.8537 | 11.0691 | 1.00 | 4.4 | Mirandola (hinge) | R | 95 | PL (Undefined) |

The values of the "depth" (expressed in metres with reference to the rotary table) and the definition of the "unit" (as defined in Fig. 3) are obtained from borehole logs data (*H* carried out for hydrocarbon explorations, *R* carried out by Regione Emilia-Romagna)

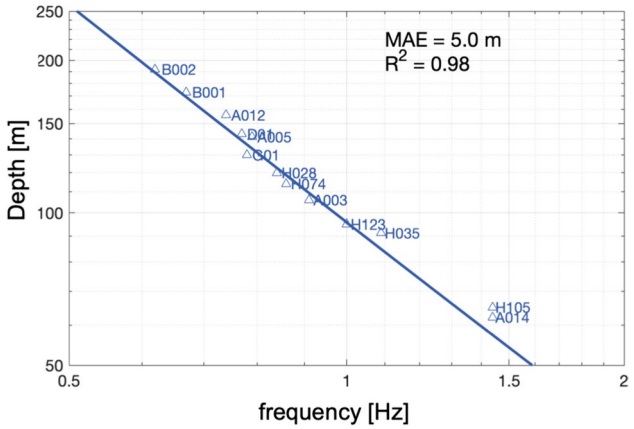


**Fig. 13** Peak frequency obtained from single-station measurements carried out in correspondence with the boreholes for which the stratigraphic log is available *versus* the depth corresponding to the identified 'resonant surface'. Further information in Table 1. The regression curve has been used for depth 'conversion' of all the HVSR peak frequencies

information derived from boreholes and seismic reflection profiles carried out for hydrocarbon purposes.

Although the capacity to identify and reconstruct the geological and seismic bedrock surfaces in restricted alluvial plains by means of microtremor analysis has been clearly documented (*e.g.* Gosar and Lenart 2010; Poggi et al. 2015; Mantovani et al. 2018; Cipta et al. 2018; Mele et al. 2021; Ito et al. 2021), in large sedimentary basins and alluvial plains in Italy (Mascandola et al. 2019; Martelli 2021), Kazakhstan (Parolai et al. 2019), New Zealand (Mucciarelli 2011) and USA (Zandieh and Pezeshk 2011) this capacity is a much-debated topic generally investigated only at a large scale. In correspondence with buried structural highs, where these two surfaces coincide, the proposed approach allows modelling with good resolution the depth variations of this surface, and this information could contribute to better estimate the local seismic response and its lateral variations. In this regard, maps showing the distribution of resonance frequencies, combined with the corresponding HVSR amplitude values, are of utmost importance for the identification of areas characterized by high impedance contrast, where greater seismic amplification is expected in case of moderate-to-strong earthquakes. It is likely that many other regions where the regional subsidence rate is greater even of the 'local' uplift rate associated with growing fault-related anticlines or of normal-fault footwall blocks, and seismic hazard is not negligible could largely benefit from the systematic application of the proposed approach. For example, these could be the Lower Rhine Graben, the Lower Tagus Valley, the Eastern Tennessee Seismic zone, the Gangetic plain, among many others worldwide. Considering also the very low cost of both necessary technology and fieldwork time, the potential advantages in terms of geological knowledge could be important.

Based on the above, the major results of the present research could be synthetized as follows:

1. The systematic application of HVSR over a dense grid allows the identification of, *e.g.*, folded surfaces related to active tectonic structures;

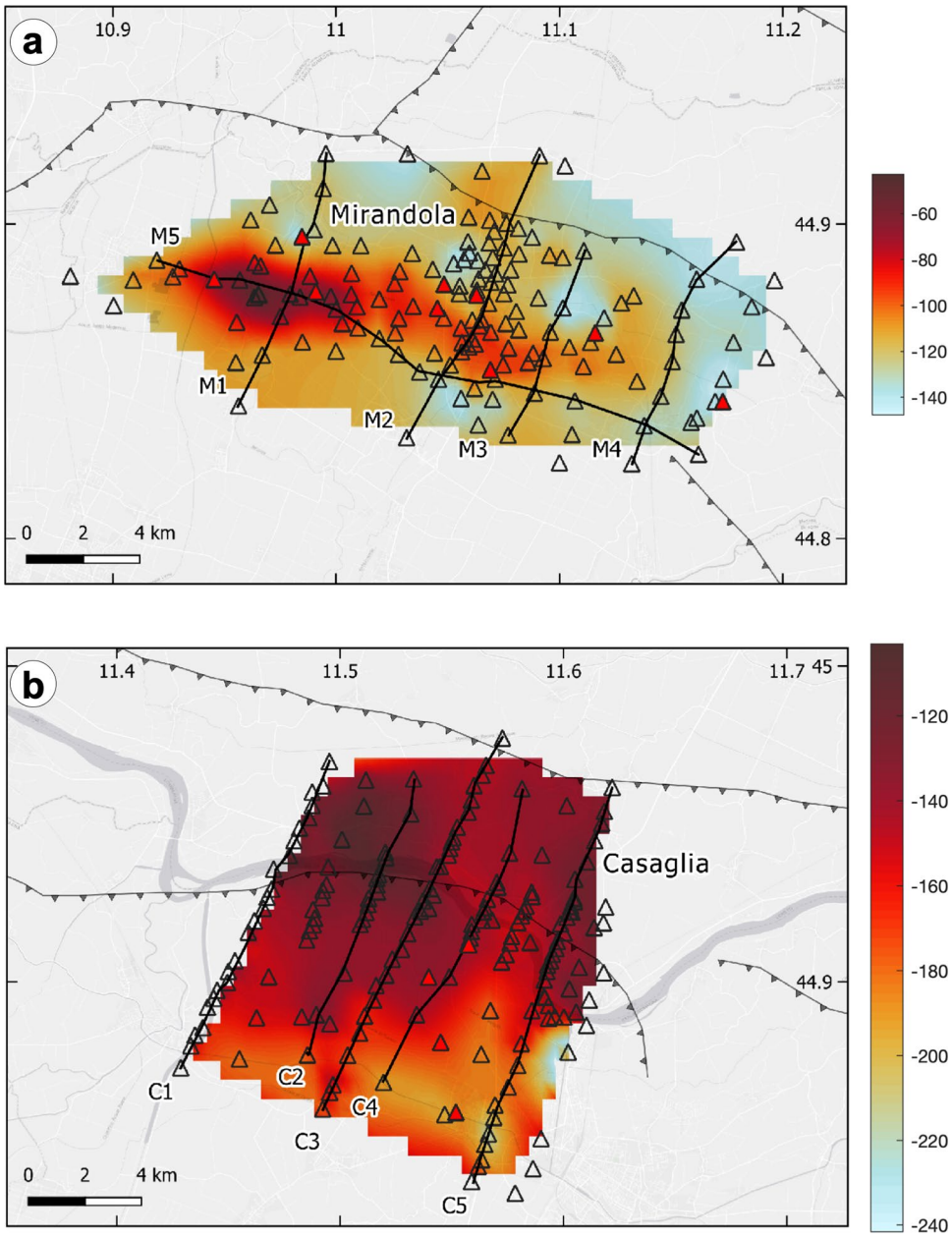


**Fig. 14** Depth maps interpolated from the values obtained using the frequency-depth regression model (Fig. 13) applied to the entire HVSR dataset in Mirandola (**a**) and Casaglia (**b**) areas

2. This is not always reflected in spatial changes of frequencies due to the complex stratigraphy of the Po Plain;
3. The real proxy seems to be the occurrence of a large amplitude anomaly in a narrow area;
4. A large-scale study with sparse data could prevent a sufficient geometrical reconstruction of these features and in the worst case even their identification;
5. The geometrical reconstruction and quantification of the amplitude anomaly is crucial for seismic site response modelling;
6. The availability of a borehole dataset may allow the definition of peak frequency *versus* depth relationship and 2D/3D modelling.

**Supplementary Information** The online version contains supplementary material available at https://doi.org/10.1007/s00531-024-02448-0.

**Acknowledgements** We wish to thank Luca Martelli and Alberto Riva for the fruitful discussions and Andrea De Biasi and Mirko Bonazza for their important contribution in the field measurements.

**Funding** Open access funding provided by Istituto Nazionale di Geofisica e Vulcanologia within the CRUI-CARE Agreement.

**Data availability** The data supporting the findings of this study are available in the Supplementary Materials. For further inquiries regarding the data, please contact the corresponding author.

## References

Albarello D, Cesi C, Eulilli V, Guerrini F, Lunedei E, Paolucci E, Pileggi D, Puzzilli LM (2011) The contribution of the ambient vibration prospecting in seismic microzoning: an example from the area damaged by the april 6, 2009 L'Aquila (Italy) earthquake. Boll Geof Teor Appl 52(3):513–538. https://doi.org/10.4430/bgta0013

Bard PY, Acerra C, Alguacil G, Anastasiadis A, Atakan K, Azzara R, Basili R, Bertrand E, Bettig B, Blarel F, Bonnefoy-Claudet S, Bordoni P, Borges A, Bøttger-Sørensen M, Bourjot L, Cara F, Caserta A, Chatelain JL, Cornou C, Cotton F, Cultrera G, Daminelli R, Dimitriu P, Dunand F, Duval AM, Fäh D, Fojtikova L, de Franco R, Di Giulio G, Grandison M, Guéguen P, Guillier B, Haghshenas E, Havskov J, Jongmans D, Kind F, Kirsch J, Koehler A, Koller M, Kristek J, Kristekova M, Lacave C, La Rocca M, Marcellini A, Maresca R, Margaris B, Moczo P, Moreno B, Morrone A, Ohrnberger M, Ojeda JA, Oprsal I, Pagani M, Panou A, Paz C, Querendez E, Rao S, Rey J, Richter G, Rippberger J, Roquette P, Roten D, Rovelli A, Saccoroti G, Savvaidis A, Scherbaum F, Schisselé E, Spühler-Lanz E, Tento A, Teves-Costa P, Theodulidis N, Tvedt E, Utheim T, Vassiliadès JF, Vidal S, Viegas G, Vollmer D, Wathelet M, Woessner J, Wolff K, Zacharapoulos S (2005) Guidelines for the implementation of the H/V spectral ratio technique on ambient vibrations measurements, processing and interpretation. Deliverable D23.12 of the SESAME project, pp. 62, April 2005. http://www.SESAME-FP5.obs.ujf-grenoble.fr

Bigi G, Bonardini G, Catalano R, Cosentino D, Lentini F, Parotto M, Sartori R, Scandone P, Turco E (1992) Structural model of Italy, 1:500,000. Consiglio Nazionale delle Ricerche, Rome

Boccaletti M, Bonini M, Corti G, Gasperini P, Martelli L, Piccardi L, Tanini C, Vannucci G (2004) Seismotectonic Map of the Emilia-Romagna Region, 1:250000. Regione Emilia-Romagna—CNR.

Bonnefoy-Claudet S, Cotton F, Bard P (2006) The nature of noise wavefield and its applications for site effects stud- ies: a literature review. Earth-Sci Rev 79(3–4):205–227. https://doi.org/10.1016/j.earscirev.2006.07.004

Burrato P, Ciucci F, Valensise G (2003) An inventory of river anomalies in the Po Plain, Northern Italy: evidence for active blind thrust faulting. Ann Geophys 46(5):865–882. https://doi.org/10.4401/ag-3459

Burrato P, Vannoli P, Fracassi U, Basili R, Valensise G (2012) Is blind faulting truly invisible? Tectonic-controlled drainage evolution in the epicentral area of the May 2012, Emilia-Romagna earthquake sequence (northern Italy). Ann Geophys 55(4):525–531. https://doi.org/10.4401/ag-6182

Caputo R, Tarabusi G (2016) Il complesso sistema di sorgenti sismogeniche nell'area ferrarese e i loro effetti nella storia. Accademia Delle Scienze Di Ferrara, Atti 93:166–177

Caputo R, Pellegrinelli A, Bignami C, Bondesan A, Mantovani A, Stramondo S, Russo P (2015) High-precision levelling, DInSAR and geomorphological effects in the Emilia 2012 epicentral area. Geomorph 235:106–117. https://doi.org/10.1016/j.geomorph.2015.02.002

Castellaro S (2016) The complementarity of H/V and dispersion curves. Geophysics 81(6):T323–T338. https://doi.org/10.1190/geo2015-0399.1

Castellaro S, Mulargia F (2009) $V_{s30}$ estimates using constrained H/V measurements. Bull Seism Soc Am 99:761–773. https://doi.org/10.1785/0120080179

Castellaro S, Mulargia F, Bianconi L (2005) Passive seismic stratigraphy: a new efficient, fast and economic technique. J Geotech Environ Geol 3:51–77

Cenni N, Viti M, Baldi P, Mantovani E, Bacchetti M, Vannucchi A (2013) Present vertical movements in Central and Northern Italy from GPS data: possible role of natural and anthropogenic causes. J Geodyn 71:74–85. https://doi.org/10.1016/j.jog.2013.07.004

Cipta A, Cummins P, Dettmer J, Syagin E, Irsyam M, Rudyanto A, Murjaya J (2018) Seismic velocity structure of the Jakarta Basin, Indonesia, using trans-dimensional Bayesian inversion of horizontal-to-vertical spectral ratios. Geophys J Int 215:431–449. https://doi.org/10.1093/gji/ggy289

Cuffaro M, Riguzzi F, Scrocca D, Antonioli F, Carminati E, Livani M, Doglioni C (2010) On the geodynamics of the northern Adriatic plate. Rend. Fis. Acc. Lincei 21:S253–S279. https://doi.org/10.1007/s12210-010-0098-9

DISS Working Group (2021) Database of Individual Seismogenic Sources (DISS), version 3.3.0: a compilation of potential sources for earthquakes larger than M 5.5 in Italy and surrounding areas. https://doi.org/10.13127/DISS3.3.0

Ermert L, Poggi V, Fäh BJ, D, (2014) Fundamental and higher 2-D resonance modes of an Alpine valley. Geophys J Int 198(2):795–811. https://doi.org/10.1093/gji/ggu072

Famiani D, Cara F, Di Giulio G, Vassallo M, Milana G (2022) Detection of hidden faults within the Fucino basin from singlestation ambient noise measurements: the case study of the Trasacco fault system. Front Earth Sci 10:937848. https://doi.org/10.3389/feart.2022.937848

GeoMol Team (2015) GeoMol – Assessing subsurface potentials of the Alpine Foreland Basins for sustainable planning and use of natural resources, Project Report, Augsburg, LfU, p. 188 pp. https://www.geomol.eu/geomol/report/GeoMol_Report_web_reduced.pdf

Gosar A, Lenart A (2010) Mapping the thickness of sediments in the Ljubljana Moor basin (Slovenia) using microtremors. Bull Earthq Eng 8:501–518. https://doi.org/10.1007/s10518-009-9115-8

Ibs-von Seht M, Wohlenberg J (1999) Microtremor measurements used to map thickness of soft sediments. Bull Seism Soc Am 89(1):250–259

Ito E, Cornou C, Nagashima F, Kawase H (2021) Estimation of velocity structures in the Grenoble Basin, France, using pseudo earthquake horizontal-to-vertical spectral ratio from microtremors. Bull Seismol Soc Am 111(2):627–653. https://doi.org/10.1785/0120200211

Khalili M, Mirzakurdeh AV (2019) Fault detection using microtremor data (HVSR-based approach) and electrical resistivity survey. J Rock Mech Geotech Eng. https://doi.org/10.1016/j.jrmge.2018.12.003

Lermo J, Chávez-Garcia FJ (1994) Are microtremors useful in site response evaluation? Bull Seismol Soc Am 84(5):1350–1364

Livani M, Petracchini L, Benetatos C, Marzano F, Billi A, Carminati E, Doglioni C, Petricca P, Maffucci R, Codegone G, Rocca V, Verga F, Antonecchi I (2023) Subsurface geological and geophysical data from the Po Plain and the Northern Adriatic Sea (North Italy). Earth Syst Sci Data Discuss 2023:1–41. https://doi.org/10.5194/essd2023-65

Maesano FE, D'Ambrogi C, Burrato P, Toscani G (2015) Slip-rates of blind thrusts in slow deforming areas: examples from the Po

Plain. Tectonophysics 643:8–25. https://doi.org/10.1016/j.tecto.2014.12.007
Mantovani A, Valkaniotis S, Rapti D, Caputo R (2018) Mapping the palaeo-Piniada Valley, Central Greece, based on systematic microtremor analyses. Pure Appl Geophys 175(3):865–881. https://doi.org/10.1007/s00024-017-1731-7
Mantovani A, Abu Zeid N, Bignardi S, Tarabusi G, Santarato G, Caputo R (2019) Seismic noise-based strategies for emphasizing recent tectonic activity and local site effects: the Ferrara Arc, Northern Italy, case study. Pure Appl Geophys 176(6):2321–2347. https://doi.org/10.1007/s00024-019-02120-8
Martelli L (2021) Assessment of seismic bedrock in deep Alluvial Plains. Case studies from the Emilia-Romagna Plain. Geosciences 11(7):297. https://doi.org/10.3390/geosciences11070297
Mascandola C, Massa M, Barani S, Albarello D, Lovati S, Martelli L, Poggi V (2019) Mapping the seismic bedrock of the Po Plain (Italy) through ambient-vibration monitoring. Bull Seism Soc Am 109(1):164–177. https://doi.org/10.1785/0120180193
Mele M, Bersezio R, Bini A, Bruno M, Giudici M, Tantardini D (2021) Subsurface profiling of buried valleys in central alps (northern Italy) using HVSR single-station passive seismic. J Appl Geophys 193:104407. https://doi.org/10.1016/j.jappgeo.2021.104407
Mi B, Hu Y, Xia J, Socco LV (2019) Estimation of horizontal-to-vertical spectral ratios (ellipticity) of Rayleigh waves from multistation active-seismic records. Geoph 84(6):EN81–EN92. https://doi.org/10.1190/geo2018-0651.1
Minarelli L, Amoroso S, Tarabusi G, Stefani M, Pulelli G (2016) Down-hole geophysical characterization of middle-upper quaternary sequences in the Apennine Foredeep, Mirabello. Italy Ann Geophys 59(5):7. https://doi.org/10.4401/ag-7114
Mistroni L (2016) Interpretazione di un profilo sismico attraverso l'Arco di Ferrara centrale. MSc thesis, University of Ferrara, pp. 58 (unpublished).
Moisidi M, Vallianatos F, Kershaw S, Collins P (2015) Seismic site characterization of the Kastelli (Kissamos) basin in northwest Crete (Greece): assessments using ambient noise recordings. Bull Earthq Eng 13:725–753. https://doi.org/10.1007/s10518-014-9647-4
Mucciarelli M (2011) Ambient noise measurements following the 2011 Christchurch earthquake: relationships with previous microzonation studies, liquefaction, and nonlinearity. Seism Res Letts 82(6):919–926. https://doi.org/10.1785/gssrl.82.6.919
Nakamura Y (1989) A method for dynamic characteristics estimation of subsurface using microtremor on the ground surface. Quart Rep Railway Tech Res Inst (RTRI) 30:25–33
Oliveto AN, Mucciarelli M, Caputo R (2004) HVSR prospections in multi-layered environments: an example from the Tyrnavos Basin (Greece). J Seism 8:395–406. https://doi.org/10.1023/B:JOSE.0000038452.12593.6f
Özalaybey S, Zor E, Ergintav S, Tapirdamaz MC (2011) Investigation of 3-D basin structures in the İzmit Bay area (Turkey) by single-station microtremor and gravimetric methods. Geophys J Int 186(2):883–894. https://doi.org/10.1111/j.1365-246X.2011.05085.x
Paolucci E, Albarello D, D'Amico S, Lunedei E, Martelli L, Mucciarelli M, Pileggi D (2015) A large scale ambient vibration survey in the area damaged by may–june 2012 seismic sequence in Emilia Romagna. Italy Bull Earthquake Eng 13(11):3187–3206. https://doi.org/10.1007/s10518-015-9767-5
Parolai S, Bormann P, Milkereit C (2002) New relationships between Vs, thickness of sediments, and resonance frequency calculated by the H/V ratio of seismic noise for the Cologne area (Germany). Bull Seismol Soc Am 92(6):2521–2527. https://doi.org/10.1785/0120010248
Parolai S, Maesano FM, Basili R, Silacheva N, Boxberger T, Pilz M (2019) Fingerprint identification using noise in the horizontal-to-vertical spectral ratio: retrieving the impedance contrast structure for the Almaty Basin (Kazakhstan). Front Earth Sci 7:336. https://doi.org/10.3389/feart.2019.00336
Pieri M, Groppi G (1981) Subsurface geological structure of the Po Plain. Consiglio Nazionale delle Ricerche, Progetto finalizzato Geodinamica, sottoprogetto Modello Strutturale, pubbl., Roma
Poggi V, Ermert L, Burjanek J, Michel C, Fah D (2015) Modal analysis of 2-D sedimentary basin from frequency domain decomposition of ambient vibration array recordings. Geophys J Int 200:615–626. https://doi.org/10.1093/gji/ggu420
Pondrelli S, Salimbeni S, Perfetti P, Danecek P (2012) Quick regional centroid moment tensor solutions for the Emilia 2012 (northern Italy) seismic sequence. Ann Geophys 55(4):615–621. https://doi.org/10.4401/ag-6146
Sánchez-Sesma FJ (2017) Modeling and inversion of the microtremor H/V spectral ratio: physical basis behind the diffuse field approach. Earth Planets Space 69(1):92
Severi P, Mazzoni R, Martelli L (2021) Oil and gas activities in Emilia-Romagna Region (Italy): land deformation and territory protection. Boll Geof Teor Appl 62(2):269–278. https://doi.org/10.4430/bgta0327
Sgattoni G, Castellaro S (2020) Detecting 1-D and 2-D ground resonances with a single-station approach. Geophys J Int 223(1):471–487. https://doi.org/10.1093/gji/ggaa325
Sgattoni G, Lattanzi G, Castellaro S (2023) An experimental approach to unravel 2D ground resonances: application to an alluvial-sedimentary basin. Earth, Planets and Space 75:74. https://doi.org/10.1186/s40623-023-01825-4
Sgattoni G, Morelli C, Lattanzi G, Castellaro S, Cucato M, Cheatal W, Mair V (2024) Geophysical investigation and 3D modeling of bedrock morphology in an urban sediment-filled basin: the case of Bolzano (Northern Italy). Pure Appl Geophys 181:1871–1893. https://doi.org/10.1007/s00024-024-03512-1
Tarabusi G, Caputo R (2017) The use of HVSR measurements for investigating buried tectonic structures: the Mirandola anticline, northern Italy, as a case study. Int J Earth Sci 106(1):341–353. https://doi.org/10.1007/s00531-016-1322-3
Tün M, Pekkan E, Özel O, Guney Y (2016) An investigation into the bedrock depth in the Eskisehir Quaternary Basin (Turkey) using the microtremor method. Geophys J Int 207:589–607. https://doi.org/10.1093/gji/ggw294
Turrini C, Toscani G, Lacombe O, Roure F (2016) Influence of structural inheritance on foreland-foredeep system evolution: an example from the Po valley region (northern Italy). Mar Petrol Geol 77:376–398. https://doi.org/10.1016/j.marpetgeo.2016.06.022
Vannoli P, Burrato P, Valensise G (2015) The seismotectonics of the Po Plain (Northern Italy): tectonic diversity in a blind faulting domain. Pure Appl Geophys 172:1105–1142. https://doi.org/10.1007/s00024-014-0873-0
Yamada M, Cho I, Kuo CH, Lin CM, Miyakoshi K, Guo Y, Hayashida T, Matsumoto Y, Mori J, Yen YT, Kuo KC (2020) Shallow subsurface structure in the Hualien Basin and relevance to the damage pattern and fault rupture during the 2018 Hualien Earthquake. Bull Seismol Soc Am 110:2939–2952. https://doi.org/10.1785/0120200063
Zandieh A, Pezeshk S (2011) A study of horizontal-to-vertical component spectral ratio in the New Madrid Seismic Zone. Bull Seismol Soc Am 101(1):287–296. https://doi.org/10.1785/0120100120